A Comparison of Three Meshless Algorithms: Radial Point Interpolation, Non-Symmetric and Symmetric Kansa Method

T. Kaufmann and C. Fumeaux
School of Electrical & Electronic Engineering,
The University of Adelaide
Adelaide, South Australia 5005, Australia

C. Engström
Laboratory for Electromagnetic Fields
and Microwave Electronics (IFH),
ETH Zurich, Zurich, CH-8092, Switzerland

***Abstract*—Three different meshless methods based on radial basis functions are investigated for the numerical solution of electromagnetic eigenvalue problems. The three algorithms, the non-symmetric Kansa approach, the symmetric Kansa method and the radial point interpolation method, are first described putting emphasis on the influence of their formalism on practical implementation. The convergence rate of these meshless methods is then investigated, showing through selected examples surprisingly similar performance despite very different formulations. The most appropriate algorithm selection will then depend on efficiency and ease of implementation for the class of problems considered, i.e. eigenvalue problems, frequency-domain or time-domain. When compared to various finite-element (FE) implementations for the presented numerical examples, the meshless methods appear more accurate and efficient than the FE methods. Those results combined with the convenience of node distribution adaptation makes meshless algorithms very promising for electromagnetic simulations.**

***Index Terms*—eigenvalues and eigenfunctions, meshless methods, finite difference methods, radial basis functions.**

I. Introduction

Meshless methods are an emerging alternative to mesh-based methods in computational electromagnetics. Instead of solving differential equations numerically on a mesh topology, the problem is solved on a set of collocation nodes. This avoids the computational effort related to mesh generation and the overhead required for handling a mesh topology. Additionally, node adaptation for improving the accuracy or for optimization is greatly simplified.

Radial basis functions (RBFs) are used in this paper, instead of the polynomial basis functions typically applied in classical collocation methods. RBF collocation methods include the Kansa method [1] and the radial point interpolation method (RPIM) [2]. The use of RBFs is gaining popularity in many fields of science, e.g. neural networks or statistical analysis. Interpolation by these basis functions offers improved accuracy for flatter function shapes at the cost of increasing matrix condition numbers. For the numerical solution to partial differential equations they promise exponential convergence rates with increasing node densities and/or wider basis functions [3]. The method can be seen as a generalized finite-difference method with highly accurate solutions due to advanced basis functions. In electromagnetics, a time-domain implementation of RPIM, which was presented in 2D for first-order problems [4], has been extended to 3D [5] and to an unconditionally stable formulation [6].

In this paper we investigate two variants of the Kansa method and RPIM applied to eigenvalue problems for the second-order wave equation. The Kansa method yields a non-symmetric problem that is not necessarily well-posed. An extension has been developed in a symmetric form [7]. We develop a formulation of this well-posed symmetric Kansa method to eigenvalue problems. Both Kansa methods solve for the interpolation coefficients rather than for the field quantities directly. In contrast, the RPIM approach is adapted towards an identity mass matrix, which is advantageous for time-domain solvers.

After an overview of their general characteristics, the accuracy of the Kansa and RPIM algorithms is compared to two variants of finite-element methods (FEMs). The goal is to clarify the differences between the meshless approaches and to propose applications for each method.

II. Method

In this section we first introduce the second-order eigenvalue problem and describe the framework of interpolation by radial basis functions. Later the specific implementation of the basis functions for the three methods is summarized.

A. Second-Order Eigenvalue Problems

A two-dimensional transverse-magnetic (TM) second-order problem is considered in this paper. The scalar electric field E_z points perpendicularly to the computational domain Ω defined in the x, y-plane. A Dirichlet boundary condition is applied to model a perfect electric conductor (PEC). This yields

$$-\Delta E_z - k^2 E_z = 0 \quad \text{in } \Omega \tag{1a}$$

$$E_z = 0 \quad \text{on } \partial\Omega \tag{1b}$$

with the wavenumber k. To formulate an eigenvalue problem we define the eigenvalues $\lambda = k^2$ inside of the computational domain and write (1a) as

$$-\Delta E_z = \lambda E_z. \tag{2}$$

C. Fumeaux acknowledges the support of the Australian Research Council (ARC) Future Fellowship funding scheme (under FT100100585).
T. Kaufmann was a PhD student at ETH Zurich wenn this work was done.

978-1-61284-757-3/11/$26.00 C2011 IEEE

In discretized form this becomes

$$-\mathbf{A}\mathbf{\Phi} = \lambda \mathbf{B}\mathbf{\Phi} \tag{3}$$

with a vector $\mathbf{\Phi}$ of length equal to the number of nodes. $\mathbf{A}$ is the stiffness matrix for the Laplacian and $\mathbf{B}$ the mass matrix. By rearranging these two matrices the method can be further modified to only solve for the interior nodes using modified $\mathbf{A}'$, $\mathbf{B}'$. This step is explained later and leads to a non-singular matrix $\mathbf{B}'$.

B. Radial Basis Functions

Radial basis functions are of high interest for the interpolation of scattered data due to their high accuracy [8]. A field value u at position $\mathbf{x}$ can be approximated using basis functions at N collocation nodes $\mathbf{x}_n$ by

$$\langle u(\mathbf{x})\rangle = \sum_{n=1}^{N} a_n \phi_n(\mathbf{x}). \tag{4}$$

Here the radial basis functions are of Gaussian type

$$\phi_n(\mathbf{x}) = \exp\left(-\alpha_c \frac{|\mathbf{x}_n - \mathbf{x}|^2}{d_c^2}\right) \tag{5}$$

and centered at the collocation nodes $\mathbf{x}_n$. The accuracy of the method depends on the shape factor α_c. In general, a lower value leads to more accurate results, but also to larger condition numbers. Conversely, if the value of α_c is too large, the system becomes unstable. The sensitivity of the method on this shape parameter has been widely reported [9]. Recently an algorithm, the leave-one-out-cross-validation (LOOCV) for pseudo-spectral methods [7], has been presented that leads to high accuracy by optimizing this shape parameter. Despite the radial dependence of the basis functions, the accuracy benefits are visible on arbitrary node distributions regardless of domain shapes, as demonstrated in [10].

The RBFs applied here are globally supported, leading to full matrices. To increase the scaling properties of the method for larger problems, compactly supported basis functions like the Wendland basis functions [8] can be used or the problem could be solved in a localized approach to obtain sparse matrices [2]. Unfortunately both these options degrade accuracy. An alternative approach to maintain the accuracy of global basis functions while being able to solve large problems is the use of domain decomposition [11].

C. Non-Symmetric Kansa Method

We follow the implementation of [12] for the non-symmetric Kansa Method (NS-Kansa). There the basis functions at the boundary nodes are replaced with their gradients, which give better accuracy. The governing equation (4) subsequently becomes

$$\langle u(\mathbf{x})\rangle = \sum_{n=1}^{N_I} a_n \phi_n(\mathbf{x}) + \sum_{n=N_I+1}^{N_B} a_n (\mathbf{x}-\mathbf{x}_n)\nabla\phi_n(\mathbf{x}) \tag{6}$$

with N_I interior and N_B boundary nodes ($N = N_I + N_B$). The eigenvalue problem (2) can now be discretized and written in the matrix form (3) using

$$[\tilde{\mathbf{A}}_1^{\mathcal{L}}]_{i,j} = \Delta\phi_j(\mathbf{x}_i), \qquad \begin{cases} i = [1, N_I] \\ j = [1, N_I] \end{cases} \tag{7a}$$

$$[\tilde{\mathbf{A}}_1^{\mathcal{L}\nabla}]_{i,j} = \Delta(\mathbf{x}_i - \mathbf{x}_j)\nabla\phi_j(\mathbf{x}_i), \begin{cases} i = [1, N_I] \\ j = [N_I+1, N_B] \end{cases} \tag{7b}$$

$$[\tilde{\mathbf{A}}_1]_{i,j} = \phi_j(\mathbf{x}_i), \qquad \begin{cases} i = [N_I+1, N_B] \\ j = [1, N_I] \end{cases} \tag{7c}$$

$$[\tilde{\mathbf{A}}_1^{\nabla}]_{i,j} = (\mathbf{x}_i - \mathbf{x}_j)\nabla\phi_j(\mathbf{x}_i), \quad \begin{cases} i = [N_I+1, N_B] \\ j = [N_I+1, N_B] \end{cases} \tag{7d}$$

$$[\tilde{\mathbf{B}}_1]_{i,j} = \phi_j(\mathbf{x}_i), \qquad \begin{cases} i = [1, N_I] \\ j = [1, N_I] \end{cases} \tag{7e}$$

$$[\tilde{\mathbf{B}}_1^{\nabla}]_{i,j} = (\mathbf{x}_i - \mathbf{x}_j)\nabla\phi_j(\mathbf{x}_i), \quad \begin{cases} i = [N_I+1, N_B] \\ j = [1, N_B] \end{cases} \tag{7f}$$

The stiffness and mass matrices (3) are given by

$$\mathbf{A}_1 = \begin{bmatrix} \tilde{\mathbf{A}}_1^{\mathcal{L}} & \tilde{\mathbf{A}}_1^{\mathcal{L}\nabla} \\ \tilde{\mathbf{A}}_1 & \tilde{\mathbf{A}}_1^{\nabla} \end{bmatrix}, \quad \mathbf{B}_1 = \begin{bmatrix} \tilde{\mathbf{B}}_1 & \tilde{\mathbf{B}}_1^{\nabla} \\ \mathbf{0} & \end{bmatrix}. \tag{8}$$

The problem size can be reduced by reforming the lower blocks of $\mathbf{A}_1, \mathbf{B}_1$ and inserting them into the upper part [12].

$$\mathbf{A}_1' = \left[\tilde{\mathbf{A}}_1^{\mathcal{L}} - \tilde{\mathbf{A}}_1^{\mathcal{L}\nabla}\,\tilde{\mathbf{A}}_1^{-1}\tilde{\mathbf{A}}_1^{\nabla}\right], \quad \mathbf{B}_1' = \left[\tilde{\mathbf{B}}_1 - \tilde{\mathbf{B}}_1^{\nabla}\,\tilde{\mathbf{A}}_1^{-1}\tilde{\mathbf{A}}_1^{\nabla}\right] \tag{9}$$

We solve (3) for the interpolation coefficients $\mathbf{\Phi} = [a_1, \ldots, a_{N_I}]^T$. The extraction of the field values is done via (6) and involves a matrix inversion. The $N_I \times N_I$ matrices $\mathbf{A}'$, $\mathbf{B}'$ are not symmetric and counter examples show that $\mathbf{A}'$ may not be invertible [13]. However, it should be noted that for a large number of investigated numerical examples this did not cause any adverse effect on the results [14]. A thorough theoretical investigation on this issue was performed in [15] and is was shown that it generally can be solved through oversampling.

D. Symmetric Kansa Method

The formulation of the NS-Kansa method can be brought to a symmetric form by modification of the basis functions. The Gaussian interior RBFs ϕ_n are replaced by their Laplacians $\Delta^{\mathbf{x}_n}\phi_n$ where the derivatives act on the collocation nodes $\mathbf{x}_n$

$$\langle u(\mathbf{x})\rangle = \sum_{n=1}^{N_I} a_n (\Delta^{\mathbf{x}_n}\phi_n)(\mathbf{x}) + \sum_{n=N_I+1}^{N_B} a_n \phi_n(\mathbf{x}). \tag{10}$$

The stiffness and mass matrices can be constructed in the same way as for the NS-Kansa Method. Here, the Laplace operator is applied analogously as in (7a) onto the interior nodes ($\tilde{\mathbf{A}}_2^{\mathcal{L}\Delta^{\mathbf{x}_n}}$) and leads to fourth-order derivatives of the original RBFs $\Delta(\Delta^{\mathbf{x}_n}\phi_n)(\mathbf{x})$. The operator applied to the boundary nodes yields $\tilde{\mathbf{A}}_2^{\mathcal{L}}$ with $\Delta\phi_n(\mathbf{x})$ similar to (7b). The RBFs $\Delta^{\mathbf{x}_n}\phi_n$ applied to (7c) and (7e) lead to $\tilde{\mathbf{A}}_2^{\Delta^{\mathbf{x}_n}}$ and $\tilde{\mathbf{B}}_2^{\Delta^{\mathbf{x}_n}}$, respectively. The basis functions in (7d) and (7f) replaced with ϕ_n yield $\tilde{\mathbf{A}}_2$ and $\tilde{\mathbf{B}}_2$. The problem (3) becomes:

$$\mathbf{A}_2 = \begin{bmatrix} \tilde{\mathbf{A}}_2^{\mathcal{L}\Delta^{\mathbf{x}_n}} & \tilde{\mathbf{A}}_2^{\mathcal{L}} \\ \tilde{\mathbf{A}}_2^{\Delta^{\mathbf{x}_n}} & \tilde{\mathbf{A}}_2 \end{bmatrix}, \quad \mathbf{B}_2 = \begin{bmatrix} \tilde{\mathbf{B}}_2^{\Delta^{\mathbf{x}_n}} & \tilde{\mathbf{B}}_2 \\ \mathbf{0} & \end{bmatrix}. \tag{11}$$

Due to the expansion (10), the stiffness matrix $\mathbf{A}_2$ is now of symmetric form. The same transformation as in NS-Kansa brings both matrices into non-singular form:

$$\mathbf{A}_2' = \left[\tilde{\mathbf{A}}_2^{\mathcal{L}\Delta^{\mathbf{x}_n}} - \tilde{\mathbf{A}}_2^{\mathcal{L}}\,\tilde{\mathbf{A}}_2^{-1}\tilde{\mathbf{A}}_2^{\Delta^{\mathbf{x}_n}}\right], \mathbf{B}_2' = \left[\tilde{\mathbf{B}}_2^{\mathcal{L}} - \tilde{\mathbf{B}}_2\tilde{\mathbf{A}}_2^{-1}\tilde{\mathbf{A}}_2^{\Delta^{\mathbf{x}_n}}\right] \tag{12}$$

978-1-61284-757-3/11/$26.00 C2011 IEEE

Now both the mass matrix $\mathbf{A}_2$ and the stiffness matrix $\mathbf{B}_2$ are symmetric and non-singular, thus making the formulation well-posed. Additionally this symmetric form is beneficial for numerical solvers.

E. Radial Point Interpolation Method

In both Kansa methods the field quantities are extracted in a post-processing step by a matrix inversion. For RPIM, this step is moved to a preprocessing step. The basis functions here are evaluated in a point-matching procedure and a set of shape functions functions is obtained as [10]

$$\begin{aligned}\langle u(\mathbf{x})\rangle &= [\phi_1(\mathbf{x})\dots\phi_n(\mathbf{x})]\mathbf{R}_0^{-1}\mathbf{U}_s \\ &= \mathbf{\Psi}(\mathbf{x})\mathbf{U}_s = \sum_{n=1}^{N}\Psi_n(\mathbf{x})u(\mathbf{x}_n).\end{aligned} \tag{13}$$

The symmetric matrix $\mathbf{R}_0$ contains the basis functions $\phi_n(\mathbf{x})$ evaluated at all collocation node positions in the point-matching technique, and therefore $\Psi_n(\mathbf{x})$ fulfills the delta property. In contrast to the previous algorithms, a field quantity is approximated by a direct linear combination of the values at the surrounding nodes. The discretized form of (3) is obtained analogously to the previous two approaches, but this time the Laplace operator is applied to the shape function $\Psi_n(\mathbf{x})$. In order to solve the problem on the interior nodes and to bring the mass matrix into non-singular form, shape functions are only evaluated at the interior points

$$[\mathbf{A}'_3]_{i,j} = \Delta\Psi_j(\mathbf{x}_i), \qquad \begin{cases} i=[1,N_I] \\ j=[1,N_I] \end{cases} \tag{14a}$$

$$[\mathbf{B}'_3]_{i,j} = \Psi_j(\mathbf{x}_i), \qquad \begin{cases} i=[1,N_I] \\ j=[1,N_I] \end{cases}. \tag{14b}$$

The eigenfunctions $\mathbf{\Phi} = [u_1,\dots,u_{N_I}]^T$ in (3) now correspond directly to the field values. It is interesting to note that $\mathbf{B}'_3$ is the identity matrix. This is advantageous for the numerical eigenvalue solver or when the method is applied to time-domain problems, where an explicit time stepping, e.g. in the localized approach [4], leads to an efficient scheme.

III. Numerical Comparison

Numerical experiments are performed to compare the performances of the three methods. The convergence behavior for a fixed node distribution and decreasing values of the shape parameter (A) and the convergence rate for an increased node density (B) are evaluated. This is done analogously to [16] where the RPIM first-order Maxwell eigenvalue solver was considered. Fig. 1 shows the structures of the stiffness and mass matrices for the three methods. It can be seen that both Kansa mass matrices in Fig. 1a and 1b are full, whereas the mass matrix for RPIM is the identity matrix (Fig. 1c). Additionally Fig. 1b illustrates the symmetry of the structure in the S-Kansa method.

A. Parameter Convergence

A numerical experiment has been performed for a cylinder with radius one. The nodes were placed homogeneously in a concentric fashion with five nodes per radius. This results in a matrix size of 79×79. According to [3], the accuracy

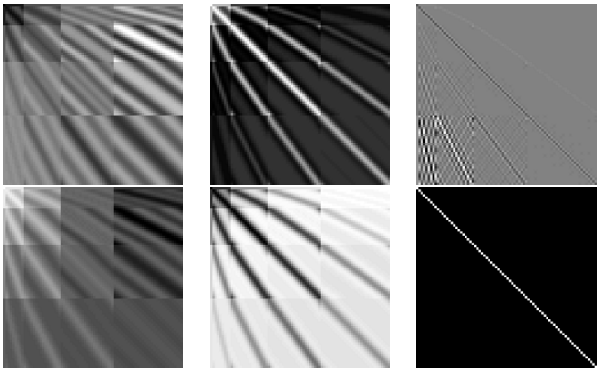

(a) (b) (c)

Fig. 1. Matrix structures for (a) the non-symmetric Kansa Method (9), (b) the symmetric Kansa Method (12) and (c) RPIM (14). The stiffness matrix $\mathbf{A}'$ is shown on top and the mass matrix $\mathbf{B}'$ on the bottom.

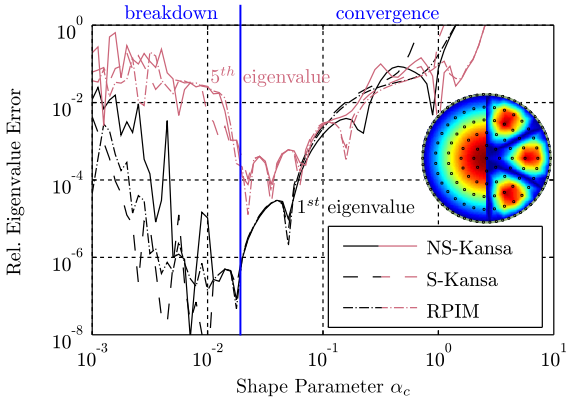

Fig. 2. Convergence for decreasing values of the shape parameter α_c. The number of degrees of freedom is fixed to $n_{dof} = 79$. The node distribution is shown in the inset with the first and fifth eigenmode on the left and right, respectively.

of the methods should increase for lower values of the shape parameter α_c. This is clearly visible in Fig. 2 where the relative error for the first and fifth eigenvalues decrease down to very low minimum of 10^{-7} and 10^{-5} respectively. At a certain point, indicated by a blue line, a numerical breakdown occurs due to the ill-condition of the matrices. The results of all three RBF methods are almost identical despite the differences in the formulation.

B. Spatial Convergence

To evaluate the convergence rate and achievable accuracy of the method the error for the previous two eigenvalues has been calculated for increasing node densities. For each node distribution, the LOOCV algorithm is applied to find an optimized shape parameter α_c. Fig. 3 shows the result of the uniform refinement in the cylindrical domain. The meshless approaches show the expected exponential convergence up to a point where the rate slows down, marked by a blue line. This is explained by the inability of the current LOOCV implementation to find the best global shape parameter α_c for these larger node distributions. Again, all three RBF methods are almost identical. It should be noted that the convergence rate could be further increased by an adaptive refinement.

978-1-61284-757-3/11/$26.00 C2011 IEEE

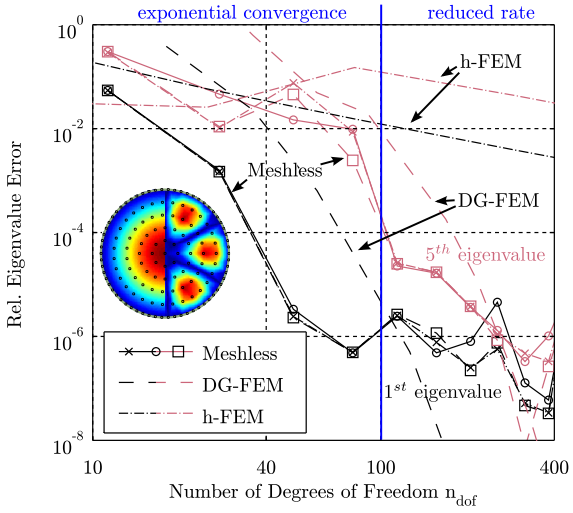

Fig. 3. Convergence for increased node densities with uniform refinement. Comparison with first-order h-FEM and high-order discontinuous Galerkin finite element-method using curved boundaries. The meshless methods are NS-Kansa (solid —o—), S-Kansa (dashed - □—) and RPIM (dash-dot -·×·-).

TABLE I
NUMBER OF DEGREES OF FREEDOM REQUIRED TO ACHIEVE AN ERROR BELOW 10^{-5} FOR THE FIRST AND FIFTH EIGENVALUE (EV).

EV	Meshless	h-FEM ($p = 1$)	h-FEM ($p = 5$)	p-DG-FEM
1	42	$1.0 \cdot 10^5$	116	92
5	170	$1.1 \cdot 10^6$	320	220

The results are compared to the first-order FEM implementation (h-FEM) in the partial differential toolbox in MATLAB and to a high-order discontinuous Galerkin (p-DG-FEM) implementation [17] with curved elements. These two methods are representative for the simplest and one of the most advanced FEM implementations available. In h-FEM, a gradual mesh refinement has been performed, and in p-DG-FEM, the polynomial order of the method has been increased step-by-step. In all cases, the meshless methods are more accurate and more efficient than the FEM implementations.

A further comparison is presented in Tab. I, where the numbers of degrees of freedom, i.e. the matrix sizes necessary to achieve a relative error of 10^{-5} are listed. An additional result has been included with a fifth-order finite-element simulation performed in COMSOL with mesh refinement. The meshless approaches outperform all three FEM codes in terms of numbers of degrees of freedom and computation time. It can also be seen that the fifth-order FEM lies in between first-order FEM and p-DG-FEM .

IV. CONCLUSION

Three meshless methods based on radial basis functions have been presented. The NS-Kansa method leads to a non-symmetric form and does not necessarily guarantee unique solutions. Brought into symmetric form, the method becomes well-posed (S-Kansa). Both algorithms solve for the interpolation coefficient and to obtain the field values, a matrix inversion is performed in the end. The radial point interpolation (RPIM) method performs this step in preprocessing where an identity mass matrix is the result.

Despite the different formulations, all algorithms appear to yield numerically almost identical results, and all methods outperform classical finite-element approaches for the presented examples. In time domain schemes where an explicit mass matrix is required RPIM is most suited. The S-Kansa method is beneficial in its ability to guarantee unique solutions. Nevertheless, for the NS-Kansa method the approach of oversampling the collocation nodes can be of use. The meshless radial basis functions represent a very promising class of numerical methods for electromagnetic simulations, as they have demonstrated a very high accuracy even for very coarse discretizations.

REFERENCES

[1] E. Kansa, "Multiquadrics – A scattered data approximation scheme with applications to computational fluid-dynamics – I surface approximations and partial derivative estimates," *Computers & Mathematics with Applications*, vol. 19, no. 8-9, pp. 127–145, 1990.

[2] G. Liu, *Mesh Free Methods: Moving Beyond the Finite Element Method*. Boca Raton, FL, USA: CRC Press, 2003.

[3] A. H.-D. Cheng, M. A. Golberg, E. J. Kansa, and G. Zammito, "Exponential convergence and H-c multiquadric collocation method for partial differential equations," *Numerical Methods for Partial Differential Equations*, vol. 19, no. 5, pp. 571–594, 2003.

[4] T. Kaufmann, C. Fumeaux, and R. Vahldieck, "The Meshless Radial Point Interpolation Method for Time-Domain Electromagnetics," in *IEEE MTT-S International Microwave Symposium Digest*. Atlanta, GA, USA: IEEE, Jun. 2008, pp. 61–65.

[5] Y. Yu and Z. D. Chen, "A 3-D Radial Point Interpolation Method for Meshless Time-Domain Modeling," *IEEE Trans. Microwave Theory and Techn.*, vol. 57, no. 8, pp. 2015–2020, Aug. 2009.

[6] ——, "Towards the Development of an Unconditionally Stable Time-Domain Meshless Method," *IEEE Trans. Microwave Theory and Techn.*, vol. 58, no. 3, pp. 578–586, Mar. 2010.

[7] G. E. Fasshauer, *Meshfree Approximation Methods with MATLAB*. River Edge, NJ, USA: World Scientific Publishing Co., Inc., 2007.

[8] M. D. Buhmann, *Radial Basis Functions: Theory and Implementations*. Cambridge, United Kingdom: Cambridge University Press, 2003.

[9] G. E. Fasshauer and J. Zhang, "On choosing "optimal" shape parameters for RBF approximation," *Numerical Algorithms*, vol. 45, no. 1, pp. 345–368, August 2007.

[10] T. Kaufmann, C. Engström, and C. Fumeaux, "Residual-Based Adaptive Refinement for Meshless Eigenvalue Solvers," in *International Conference in Electromagnetics on Advanced Applications*. Sydney, Australia: IEEE, Sep. 2010, pp. 244–247.

[11] J. Li and Y. C. Hon, "Domain decomposition for radial basis meshless methods," *Numerical Methods for Partial Differential Equations*, vol. 20, no. 3, pp. 450–462, 2004.

[12] P.-L. Jiang, S.-Q. Li, and C. H. Chan, "Analysis of elliptical waveguides by a meshless collocation method with the Wendland radial basis functions," *Microwave and Optical Technology Letters*, vol. 32, no. 2, pp. 162–165, 2002.

[13] Y. C. Hon and R. Schaback, "On unsymmetric collocation by radial basis functions," *Applied Mathematics and Computation*, vol. 119, no. 2-3, pp. 177–186, 2001.

[14] S. A. Sarra, "A numerical study of the accuracy and stability of symmetric and asymmetric RBF collocation methods for hyperbolic PDEs," *Numerical Methods for Partial Differential Equations*, vol. 24, no. 2, pp. 670–686, 2008.

[15] R. Schaback, "Convergence of Unsymmetric Kernel-Based Meshless Collocation Methods," *SIAM Journal on Numerical Analysis*, vol. 45, no. 1, pp. 333–351, 2007.

[16] T. Kaufmann, C. Engström, C. Fumeaux, and R. Vahldieck, "Eigenvalue Analysis and Longtime Stability of Resonant Structures for the Meshless Radial Point Interpolation Method in Time Domain," *IEEE Trans. Microwave Theory and Techn.*, vol. 58, no. 12, pp. 3399–3408, December 2010.

[17] C. Engström and M. Wang, "Complex dispersion relation calculations with the symmetric interior penalty method," *International Journal for Numerical Methods in Engineering*, vol. 84, no. 7, pp. 849–863, 2010.

978-1-61284-757-3/11/$26.00 C2011 IEEE